

Characterization and Mitigation of Crosstalk in Quantum Error Correction

Zeyuan Zhou^{1,2}, Andrew Ji³, and Yongshan Ding^{1,2,4}

¹*Department of Computer Science, Yale University, New Haven, CT 06511*

²*Yale Quantum Institute, New Haven, CT 06511*

³*University of Chicago Laboratory Schools, Chicago, IL*

⁴*Department of Applied Physics, Yale University, New Haven, CT 06520*

The design and performance analysis of quantum error correction (QEC) codes are often based on incoherent and independent noise models since it is easy to simulate. However, these models fail to capture realistic hardware noise sources, such as correlated errors (crosstalk), which can significantly impact QEC code performance, especially when they occur between data and ancillary qubits. In this paper, we systematically study various types of crosstalk noise and quantify their effects on surface codes through memory and stability experiments. Based on our findings, we introduce crosstalk-robust implementations of QEC via redundant stabilizer checks and flag qubit designs. In addition, we analyze logical crosstalk in an $[[n, k > 1, d]]$ code block and establish analytical conditions under which physical crosstalk does not lead to logical crosstalk. Together, our analytical and numerical results shed light on designing QEC codes that are robust against hardware-realistic noise, paving the way for reliable experimental realization of fault-tolerant quantum computing.

INTRODUCTION

Quantum error correction (QEC) emerges as a crucial component to realize large-scale fault-tolerant quantum computing (FTQC) [1, 2]. QEC encodes quantum information into a larger Hilbert space, which allows for detection and correction via repetitive measurements of its stabilizers. Traditionally, QEC studies assume an independent and incoherent noise model for stabilizer design and threshold simulation [1]. This model, however, falls short in capturing all error properties of a physical system. For example, correlated error, also known as crosstalk, is a detrimental realistic noise on hardware.

Generally characterized as an unwanted interaction, crosstalk takes various forms in hardware architectures. For example, in superconducting and semiconductor platforms, qubits are susceptible to parasitic ZZ interaction from always-on coupling between neighboring qubits [3–6]. In trapped-ion systems, unwanted XX -type interactions are commonly seen in the implementation of multi-qubit gates, such as the Mølmer–Sørensen gate [7–9]. Neutral atom systems also experience crosstalk when atom blockades are brought together to implement entangling gates [10, 11]. While crosstalk suppression has been thoroughly studied from both the hardware-level (e.g. coupler and gate design [12–14]) and the software-level (e.g. compiling/mapping [15–21], pulse design [22–27]), the investigation of its impact on QEC [8, 28–34] is still limited to certain platform-specific crosstalk type and lacks general measures to mitigate crosstalk.

Here, we provide a comprehensive analysis of the robustness of surface code, one of the most practical and scalable QEC codes, towards various types of crosstalk. Specifically, we perform memory and stability experiments for each code under a “depolarizing + crosstalk” noise model, from which we find the effect of crosstalk on both state preservation and fault-tolerant logical opera-

tion. Both crosstalk and depolarizing noise models are circuit-level and are inspired by state-of-the-art qubits calibration and device connectivity data. Specifically, we survey through four types of crosstalk on two dimensions: gate-based or always-on, and between data-data qubits or between data-ancilla qubits. Numerical results show that among all four types, gate-based crosstalk between data and ancilla qubits poses the most detrimental effect on both memory and FTQC. To address this issue, we propose two schemes: a redundant stabilizer check method suitable for repetition code and a flagged syndrome extraction design for surface code. Both measures enable effective detection of crosstalk and are hardware agnostic, which means gate optimization or engineering is not required. The schemes are also generalizable to more codes.

We also introduce for the first time “logical crosstalk” in an $[[n, k > 1, d]]$ code block. We show that physical crosstalk can be converted to logical correlated errors contingent on the definition of logical Pauli operators. We show how logical crosstalk could impact logical gates using $[[4, 2, 2]]$ and $[[8, 3, 2]]$ codes as examples [35, 36]. Besides, we show analytically that on a 2D sparse connectivity, logical crosstalk will not happen with large d . Together, these results fill the gap in the studies of how crosstalk impacts the instantiation of QEC and provide novel approaches to enhance crosstalk robustness.

NOISE MODEL

We simulate a circuit-level noise model including both depolarizing and crosstalk noise. For depolarizing noise, we assume that after each logical gate or reset operation, an incoherent Pauli error is inserted with an associated probability that is parametrized with a single p . We scale p from 10^{-3} to 10^{-2} in simulation. Additionally, we de-

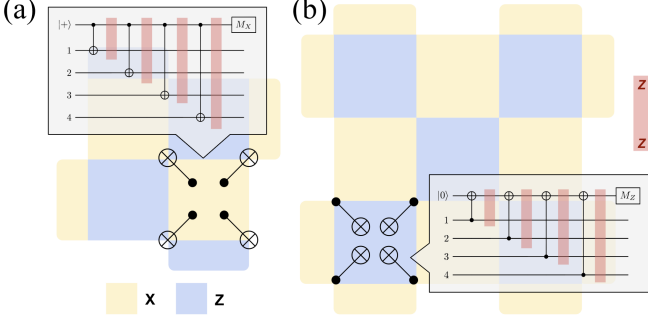


FIG. 1: The rotated surface code patch (a) and the stability experiment patch (b). The yellow (blue) plaquettes are $X(Z)$ stabilizer with support on data qubits at the vertices, and the check qubits are placed in the middle. Red shaded area denotes ZZ correlated crosstalk after each two-qubit gate in syndrome measurement circuits.

fine incoherent crosstalk as a correlated N -body Pauli error channel expressed as:

$$\mathcal{E}_N(\rho) = (1 - p_X)\rho + p_X \hat{P} \rho \hat{P}, \quad \hat{P} = \hat{\sigma}_i^{\otimes N}, \quad (1)$$

where $i \in \{X, Z\}$. Particularly, we consider four classes of crosstalk specified in Table I, which are relevant to current quantum hardware platforms. For example, in superconducting tunable qubit architectures, ZZ -type crosstalk is dominant during two-qubit gates. In fixed-frequency transmon qubits, crosstalk normally takes the form of always-on ZZ coupling between the nearest neighbors (N.N.) [4, 37, 38]. Similarly, in trapped-ion systems, residual XX -type coupling exists when implementing two-qubit gates [7–9]. We categorize them as either *gate-based* or *always-on* crosstalk between data and ancilla qubits. For a 2D grid connectivity, when syndrome extraction circuit is mapped to physical qubits, data and ancilla qubits are often nearest neighbors for reducing routing overhead. Besides those N.N. interactions, crosstalk also occurs among data qubits arising from next nearest neighbor (N.N.N.) interactions or multi-qubit gates. N.N.N. coupling of ZZ -type is common in superconducting systems, although the strength can be order(s)-of-magnitude lower than N.N. coupling [39, 40]. Multi-qubit interactions are commonly seen in neutral atom platforms when atom blockade are brought together for multi-qubit gates [10, 11].

Coherence vs Incoherence

Always-on crosstalk is shown to be coherent in current quantum devices, which is hard to fully simulate. In this

paper, we consider the Pauli-twirled incoherent simulation of such crosstalk. In the setting of a code-capacity model, a great number of studies have been conducted to study the coherence in error correction and how accurate the Pauli-twirled approximation (PTA) is in quantifying the effect of coherent noise. Assuming noiseless syndrome measurement cycles, conclusions are reached from both analytical [28, 30] and numerical studies that the ratio between coherent and incoherent contributions will decay exponentially by scaling up code distance. This implies that an incoherent noise model makes a close approximation for high distances. In a circuit-level noise model, where error (including crosstalk) can occur during syndrome measurements, we analyze a simple case shown as below to demonstrate the discrepancy between incoherent and coherent channels.

Let's first consider an X -stabilizer check circuit shown in Fig 1. Ancilla qubit is initialized in $|+\rangle = \frac{1}{\sqrt{2}}(|0\rangle + |1\rangle)$ state, and the four data qubits are in some unknown entangled state $|\psi\rangle_D = \sum_{x \in \{0,1\}^4} \alpha_x |x_1 x_2 x_3 x_4\rangle$ ($|x\rangle = |x_1 x_2 x_3 x_4\rangle$), the total initial state of the system is $|\Psi\rangle_0 = \frac{1}{\sqrt{2}}(|0\rangle + |1\rangle)|\psi\rangle_D$. After four consecutive CNOTs, the state becomes $|\Psi\rangle_1 = \frac{1}{\sqrt{2}} \sum_x \alpha_x [|0\rangle |x\rangle + |1\rangle |x \oplus 1^4\rangle]$. Due to commutivity relations, all the correlated $ZZ(\theta)$ errors can be propagated to after CNOT gates. Here we applies to each (ancilla, data) pair $U_{ZZ}(\theta) = \exp[-i\frac{\theta_i}{2} Z_0 Z_i]$, and the total unitary $U_{ZZ} = \prod_{i=1}^4 \exp[-i\frac{\theta_i}{2} Z_0 Z_i]$. Since $Z_0 Z_i |p\rangle_0 |q_i\rangle_i = (-1)^{p+q_i} |p\rangle_0 |q_i\rangle_i$, the combined phase after four correlated phase errors is $\exp[-\frac{i}{2} \sum_{i=1}^4 \theta_i (-1)^{p+x_i}]$. The resulting state becomes:

$$|\Psi_2\rangle = \frac{1}{\sqrt{2}} \sum_x \alpha_x e^{i\phi(x)} [|0\rangle |x\rangle + |1\rangle |x \oplus 1^4\rangle], \quad (2)$$

where $\phi(x) = -\frac{1}{2} \sum_{i=1}^4 \theta_i (-1)^{x_i}$. Finally after the Hadamard gate on ancilla qubit, the state becomes:

$$|\Phi\rangle = \frac{1}{2} \sum_x \alpha_x e^{i\phi(x)} [|0\rangle (|x\rangle + |x \oplus 1^4\rangle) + |1\rangle (|x\rangle - |x \oplus 1^4\rangle)] \quad (3)$$

Here, the ancilla qubit picks up phases determined by the actual state from $\phi(x)$; and the phases will destructively or constructively interfere to accumulate unless trivial θ_i value. The incoherent channel, however, is a classical mixture over 16 possible subsets S , which can be expressed as:

$$\mathcal{E}_{\text{inc}}(\rho) = \sum_{S \in \{1,2,3,4\}} \left(\prod_{i \in S} p_i \right) \left(\prod_{j \notin S} [1 - p_j] \right) (Z_0 Z_S) \rho (Z_0 Z_S), \quad (4)$$

where $Z_0 Z_S = \prod_{i \in S} Z_A Z_{D_i}$, and we try to match each θ_i by setting $p_i = \sin^2(\theta_i/2)$. However, each of the 16 possible situations are independent and cannot possibly mimic the full coherent scenario, causing a discrepancy of final state on the ancilla qubit due to phase accumulation.

Similarly, for Z -stabilizer circuit, the four data qubits will accumulate phases from crosstalk in other qubit pair

due to the propagation through CNOTs, but the ancilla qubits will be unaffected by the ZZ errors since it is in the Z -basis.

Crosstalk Type	Qubit Pair	Coupling Strength (GHz)	Error Rate	Threshold [%]	$d_{\text{eff}}(d)$	$R(w)$	Error Source
Circuit-level depolarizing noise, no crosstalk	(Baseline) single-qubit, two-qubit	$p_{2Q} = p$ $p_{1Q} = 0.1p$ $p_{\text{reset}} = 2p$ $p_{\text{meas}} = 5p$	0.74	$1.94 \pm 0.02(3)$ $2.98 \pm 0.06(5)$ $3.98 \pm 0.06(7)$ $4.91 \pm 0.10(9)$			Single-qubit gate error, two-qubit gate error, reset error, and measurement readout error
Gate-based	Data-Ancilla	$p_{ZZ} = 10^{-3}$	0.63		$1.40 \pm 0.06(3)$ $2.07 \pm 0.09(5)$ $2.79 \pm 0.02(7)$ $3.57 \pm 0.01(9)$	$1.15 \pm 0.03(4)$ $1.14 \pm 0.02(6)$ $1.14 \pm 0.02(8)$	Nearest-neighbor parasitic ZZ -type interaction during entangling gates
Always-on	Data-Ancilla	$J = 10^{-5}$	0.71		$1.83 \pm 0.01(3)$ $2.79 \pm 0.01(5)$ $3.93 \pm 0.08(7)$ $4.62 \pm 0.16(9)$	$1.00 \pm 0.02(4)$ $1.00 \pm 0.01(6)$ $1.00 \pm 0.01(8)$	Nearest-neighbor coherent ZZ -rotation due to residual coupling
Gate-based	Data-Data	$p_{ZZ} = 10^{-4}$	0.66		$0.72 \pm 0.10(3)$ $1.57 \pm 0.12(5)$ $2.13 \pm 0.18(7)$ $2.86 \pm 0.20(9)$	$1.01 \pm 0.03(4)$ $0.97 \pm 0.01(6)$ $1.00 \pm 0.02(8)$	Next-nearest-neighbor ZZ interaction during simultaneous entangling gate due to unwanted resonance
Always-on	Data-Data	$J = 10^{-5}$	0.71		$1.07 \pm 0.08(3)$ $2.11 \pm 0.12(5)$ $2.94 \pm 0.15(7)$ $3.65 \pm 0.26(9)$	$0.97 \pm 0.02(4)$ $1.02 \pm 0.02(6)$ $1.00 \pm 0.01(8)$	Next-nearest-neighbor static ZZ -rotation due to 2nd order residual coupling

TABLE I: Comparison of various crosstalk types and their impact on a rotated surface code. The first row shows the baseline depolarizing noise model without crosstalk, while all subsequent rows use the same noise model plus the corresponding crosstalk type on specified qubit pair. Parameters such as coupling strength and error rates are inspired by hardware data. Memory experiments yield the code threshold and effective distance d_{eff} , where (d) indicates the code distance. The time overhead ratio R is extracted from stability experiments, with (w) specifying the patch width. The last column identifies the error source, i.e. where the crosstalk originates on hardware.

CODE PERFORMANCE

Stabilizer Codes

We briefly introduce the stabilizer formalism for defining quantum error correction codes. An $[[n, k, d]]$ code encodes k qubits of logical information with n physical qubits to distance d , enabling correction of up to $\lfloor (d-1)/2 \rfloor$ errors and detection of up to $(d-1)$ errors. The *stabilizer group* $\mathcal{S} \subseteq \mathcal{P}_n$ (Pauli group on n qubits) is generated by $\langle S_1, S_2, \dots, S_{n-k} \rangle$ such that $[S_i, S_j] = 0, \forall i, j$, where each $S_i \in \mathcal{P}_n$ is of the form $\bigotimes_{j=1}^n P_j$ with $P_j \in \{I, X, Y, Z\}$. Then we can define a complete set of orthogonal projectors $\Pi_{\vec{s}} = \prod_{i=1}^{n-k} \frac{1}{2} (I + (-1)^{s_i} S_i)$,

where $s_i \in \{0, 1\}$ is the syndrome outcome. Based on the syndrome information, a Pauli operator $R_{\vec{s}}$ can be found to map faulty state $|\phi\rangle$ back to correct codeword state $R_{\vec{s}} \Pi_{\vec{s}} |\phi\rangle$.

Our primary focus is the rotated surface code, which has been well studied both theoretically and numerically [1, 2, 41, 42], and has been demonstrated on hardware platforms with exponential error suppression capabilities [43–45]. The rotated surface code is a generalized toric code that can be implemented on a planar surface without open boundary conditions. Surface code allows correction of both X and Z errors by checking weight-4 local stabilizers. Due to its high threshold and a large number of logical gates that can be implemented, rotated surface codes arise as one of the most promising candidates for

FTQC. Rotated surface code encode $k = 1$ logical qubit using $n = d^2$ data qubits and $(d^2 - 1)$ ancilla qubits. In most surface code instantiations, data qubits are coupled to only ancilla qubits and vice versa.

Memory Experiments

With the noise model described above, we simulated the memory of surface code patches and repetition code with various distances to examine the impact of crosstalk on the threshold. We simulated surface codes with distance $d_s \in \{3, 5, 7, 9\}$ and with repeated syndrome measurements of d_s times for fault tolerance. For each circuit, we scale the depolarizing noise parameter p from 10^{-3} to 10^{-2} . The crosstalk error rate for each type is extracted from hardware data and is held constant throughout the simulation. The error parameters are specified in Table I, with gate-based crosstalk specified by an error rate following each two-qubit gate, and always-on crosstalk is parameterized with coupling strength J . The circuits are set up by the Stim package [46] and decoded with the PyMatching package via Minimum Weight Perfect Matching (MWPM) algorithms [47]. For each circuit, Monte Carlo simulation is conducted with 10^6 shots. For baseline crosstalk-free noise and each type of crosstalk, we plot the depolarizing error rate p versus logical error rate p_L and extract the threshold value (%) and the effective distance d_{eff} . Here, d_{eff} is extracted as the exponent of p in the approximate expression for p_L as $p_L \propto p^{d_{\text{eff}}}$, which can generally be understood as the minimum number of errors needed to create a logical error. From the memory experiment, we observed that among all 4 types, gate-based crosstalk between data and ancilla qubits poses the most amount of reduction in threshold value (from 0.74 to 0.63). This implies that such syndrome extraction steps are greatly degraded due to the correlated events created by such crosstalk, causing a tighter requirement for gate fidelity for fault tolerance. On the other hand, gate-based data-data crosstalk significantly shifts up the logical error rate and lower down d_{eff} due to the reason that it creates more two-qubit correlated error and hence more likely to cause a logical error. Static always-on crosstalk, either between data-ancilla or data-data, causes relatively small changes to the logical error rates. Full plots of these simulations can be found in the supplemental materials.

Stability Experiments

While memory experiments evaluate the preservation of logical states through time, they don't directly probe the impact of errors on the movement of logical observables through space. The movement of logical information through space, however, is crucial for FTQC. Here

we use stability experiments to test how crosstalk noise affects the stabilizer measurement results [48, 49], which are extensively used to determine joint logical Pauli products in lattice surgery [42, 50–52]. Stability experiments achieve this goal by checking a global invariant across space, where the product of stabilizer measurements should equal a predetermined value. We considered stability patches with width $w \times w$ where $w \in \{4, 6, 8\}$ and depolarizing noise parameter $p \in \{10^{-2}, 10^{-2.5}, 10^{-3}\}$. These patches do not encode any logical state but have one type of stabilizer being determined beforehand. In the experiments, we first prepare all data qubits in the $|0\rangle$ state, measure the stabilizer for n rounds, and finally measure data qubits in the Z computational basis. For each configuration, we compute the logical error rate p_L as a function of the number of QEC rounds n , which follows an exponential decay $p_L = Ae^{-\gamma n}$. The decay rate γ and prefactor A are obtained through linear fitting of the logarithmic form $\log(p_L) = \log(A) - \gamma n$. We perform this analysis both for circuits with and without crosstalk noise, denoted as γ_{ct} and γ_0 respectively. To quantify the impact of crosstalk, we introduce the time overhead ratio $R = \gamma_0/\gamma_{\text{ct}}$, which represents how much longer (more rounds of syndrome measurements) the circuit with crosstalk needs to run to achieve the same logical error rate as the circuit without crosstalk. For each crosstalk type, we also run depolarizing error parameter $p = 10^{-2.5}$ but across three different crosstalk strengths. A ratio greater than 1 indicates performance degradation due to crosstalk. Our results are presented here in Table I the R ratio of each type of crosstalk for each patch width w . A minimum of n measurement errors will lead to undetectable logical failure, which becomes more pronounced in the presence of crosstalk between data and ancilla qubits since ancilla flips cause measurement classification errors. This effect is particularly visible in the increasing time overhead ratio for larger crosstalk strengths. The full results and plots are available in the supplemental materials.

CROSSTALK ROBUST QEC

From the memory and stability experiments, we observe that the most detrimental crosstalk is between data and ancilla qubits, which impacts both memory experiment by decreasing its threshold value and stability experiments in lowering down the logical error rates for a given number of syndrome rounds. To address this issue caused by crosstalk-induced ancilla flips, we propose two crosstalk-robust syndrome extraction schemes: the first scheme uses redundant stabilizer checks to detect flipped ancilla qubits; and the second scheme use flagged gadget to perform two-qubit gates fault-tolerantly.

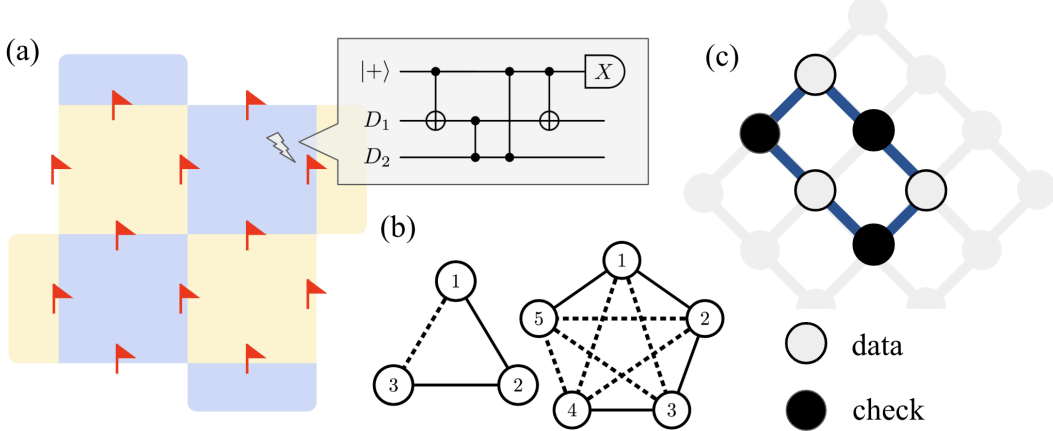


FIG. 2: Crosstalk robust quantum error correction circuit engineering. Crosstalk-flagged surface code design (a) shows where the flag qubits need to be placed and how to implement ZZ-flagged fault-tolerant CZ gates gadget between data and ancilla qubit, which involves an additional qubit to frequently measure on X-basis and reset to state $|+\rangle$. Figure (b) is a geometric representation for data qubits (vertices) and stabilizer checks (edges) in repetition codes to demonstrate the requirement of detecting erroneous edges. Figure (c) is a hardware mapping of using an extra stabilizer check for a 3-qubit repetition code. Blue lines are necessary coupling, and grey (black) circles are data (check) qubits.

Redundant Stabilizer Checks

To detect measurement classification errors, we can use redundant stabilizers to check for parity invariance across all possible stabilizer group. In a 3-qubit bit-flip code, for example, checking $s_1 = Z_1Z_2$ and $s_2 = Z_2Z_3$ provides sufficient syndrome information to decode the error on one of the three qubits. If at most 1 ancilla has error, we can introduce extra check $s_3 = Z_1Z_3$ to detect: the parity of s_1s_2 should equal s_3 . To generalize this scheme, we can formulate this problem as a graph problem: in a graph with n vertices representing n data qubits, the edges connecting them are the weight-2 stabilizer checks. For each stabilizer, to detect its error, each edge needs to be in at least one closed loop. To detect t independent ancilla errors, each one of the t edges needs to be in a distinct closed loop where the total number of erroneous edges in that loop is odd (even number of erroneous edges will be undetectable). Fig.2(b) shows a geometric representation of constructing redundant stabilizer checks for faulty ancilla qubits. And Fig.2(c) shows a 2D-grid hardware mapping for a 3-qubit repetition code with an extra stabilizer check.

Flagged Syndrome Measurement

We further propose to detect crosstalk during syndrome measurements using flag qubits for surface code, inspired from previous flag-qubit designs [53–55]. Our strategy makes use of fault-tolerant gadgets to perform crosstalk-flagged CZ gates for projective measurement,

which allows for the detection of at most 1 ZZ-type correlated error between any two qubits. Specifically, in Figure 2, between every pair of data qubits there is a flag qubit (red flag), which is coupled to both data and ancilla qubits. The triangle denotes a four-gate gadgets that performs the unitary of CZ gate between data and ancilla qubits, and the flag qubit is measured in X-basis where a -1 eigenvalue will flag a ZZ correlated error. This setup requires frequent measurement and reset of flag qubit at a rate 4 times faster than that of ancilla qubits measurements. In this setting, we also need extra flag qubits which scales with distance as $n_{\text{flag}} = 2d^2 - 2d$. Meanwhile, the number of gates needed for crosstalk-robust syndrome measurement is 4 time higher than the conventional syndrome measurement circuit (excluding measurements).

IN-PATCH LOGICAL CROSSTALK

So far we have studied how physical crosstalk can impact code performance for $[[n, k = 1, d]]$ codes. In this section we discuss the issue of logical crosstalk between logical qubits defined in a $[[n, k > 1, d]]$ code block. Start with the example of the $[[4, 2, 2]]$ error detection code, the logical Pauli operators can be defined as $\bar{Z}_1 = Z_1Z_2$ and $\bar{Z}_2 = Z_1Z_3$. Hence, if a weight-2 physical crosstalk in the form of Z_2Z_3 exists, it is being effectively converted to $\bar{Z}_1\bar{Z}_2$, a logical ZZ-type crosstalk due to the overlap of Z_1 operator that support both logical operators. Similar issue arises in the $[[8, 3, 2]]$ color code. Such a logical correlated error cannot be corrected and could affect two-

qubit gate error rates. However, here we provide a simple proof that for a $[[n, k \geq 2, d > 2]]$ code, weight-2 physical crosstalk can never be converted to logical crosstalk. And the statement can also be generalized to arbitrary weight physical crosstalk. The statement is as follows: Let \mathcal{C} be an $[[n, k, d]]$ quantum code. Suppose that physical correlated Pauli errors are at most weight- w_X . Then, for \mathcal{C} , if $d > w_X$, there will be no logical correlated Pauli error of any weight. The following is a proof sketch for the logical crosstalk condition:

Proof. Assume, for contradiction, that in the given setting there exists a logical correlated Pauli error E in the $[[n, k, d]]$ code. Since the error itself is a logical operator, its weight w_E is at least d ($w_E \geq d$). At the same time, the logical error E is converted from physical correlated error of weight $w_X = w_E \geq d$. This contradicts the setup of \mathcal{C} where $d > w_X$. Hence no logical correlated error can happen. \square

This shows that if we scale up the code distance, as long as the physical crosstalk weight is less than d , it will not be converted into a logical crosstalk error in the code block. In practice, experiments found out that the dominant crosstalk errors are weight-2 with higher-weight errors to be sufficiently small, which renders that almost any large distance code would be free from such an issue.

CONCLUSION

In this work, we have systematically investigated the impact of crosstalk noise on the performance of QEC codes, focusing on both memory and FTQC experiments. Through extensive numerical simulations, we identified gate-based crosstalk between data and ancilla qubits as the most detrimental type, significantly reducing the error threshold and increasing the time overhead ratio. To address this, we proposed two hardware-agnostic mitigation strategies: redundant stabilizer checks for repetition codes and flagged syndrome extraction for surface codes, both of which effectively detect and mitigate crosstalk-induced errors. Furthermore, we introduced the concept of logical crosstalk in multi-logical-qubit code blocks, demonstrating that physical crosstalk can propagate to logical errors under certain conditions. We provided analytical criteria to ensure that physical crosstalk does not translate into logical crosstalk, emphasizing the importance of code distance in suppressing such effects.

In summary, this work bridges the gap between theoretical QEC studies and practical hardware considerations, offering actionable insights for improving the resilience of quantum error correction in the presence of crosstalk. These results contribute to the broader goal of realizing scalable and fault-tolerant quantum computation.

ACKNOWLEDGEMENT

We would like to thank Gregory Quiroz, Pei-Kai Tsai, and Kathleen Chang for the useful discussions. This project was supported by the National Science Foundation (under award CCF-2338063). External interest disclosure: YD is a scientific advisor to, and receives consulting fees from Quantum Circuits, Inc.

- [1] D. Gottesman, Theory of fault-tolerant quantum computation, *Physical Review A* **57**, 127–137 (1998).
- [2] M. A. Nielsen and I. L. Chuang, *Quantum computation and quantum information* (Cambridge university press, 2010).
- [3] P. Krantz, M. Kjaergaard, F. Yan, T. P. Orlando, S. Gustavsson, and W. D. Oliver, A quantum engineer's guide to superconducting qubits, *Applied Physics Reviews* **6**, 021318 (2019).
- [4] A. Ash-Saki, M. Alam, and S. Ghosh, Experimental characterization, modeling, and analysis of crosstalk in a quantum computer, *IEEE Transactions on Quantum Engineering* **1**, 1 (2020).
- [5] A. Kandala, K. X. Wei, S. Srinivasan, E. Magesan, S. Carnevale, G. A. Keefe, D. Klaus, O. Dial, and D. C. McKay, Demonstration of a high-fidelity cnot gate for fixed-frequency transmons with engineered zz suppression, *Phys. Rev. Lett.* **127**, 130501 (2021).
- [6] P. Zhao, K. Linghu, Z. Li, P. Xu, R. Wang, G. Xue, Y. Jin, and H. Yu, Quantum crosstalk analysis for simultaneous gate operations on superconducting qubits, *PRX Quantum* **3**, 020301 (2022).
- [7] C. Fang, Y. Wang, S. Huang, K. R. Brown, and J. Kim, Crosstalk suppression in individually addressed two-qubit gates in a trapped-ion quantum computer, *Phys. Rev. Lett.* **129**, 240504 (2022).
- [8] P. Parrado-Rodríguez, C. Ryan-Anderson, A. Bermudez, and M. Müller, Crosstalk Suppression for Fault-tolerant Quantum Error Correction with Trapped Ions, *Quantum* **5**, 487 (2021).
- [9] C. Ospelkaus, C. E. Langer, J. M. Amini, K. R. Brown, D. Leibfried, and D. J. Wineland, Trapped-ion quantum logic gates based on oscillating magnetic fields, *Phys. Rev. Lett.* **101**, 090502 (2008).
- [10] H. Levine, A. Keesling, A. Omran, H. Bernien, S. Schwartz, A. S. Zibrov, M. Endres, M. Greiner, V. Vuletić, and M. D. Lukin, High-fidelity control and entanglement of rydberg-atom qubits, *Phys. Rev. Lett.* **121**, 123603 (2018).
- [11] E. Urban, T. A. Johnson, T. Henage, L. Isenhower, D. D. Yavuz, T. G. Walker, and M. Saffman, Observation of rydberg blockade between two atoms, *Nature Physics* **5**, 110–114 (2009).
- [12] P. Mundada, G. Zhang, T. Hazard, and A. Houck, Suppression of qubit crosstalk in a tunable coupling superconducting circuit, *Phys. Rev. Appl.* **12**, 054023 (2019).
- [13] J. Ku, X. Xu, M. Brink, D. C. McKay, J. B. Hertzberg, M. H. Ansari, and B. L. T. Plourde, Suppression of unwanted zz interactions in a hybrid two-qubit system, *Phys. Rev. Lett.* **125**, 200504 (2020).

[14] P. Zhao, P. Xu, D. Lan, J. Chu, X. Tan, H. Yu, and Y. Yu, High-contrast zz interaction using superconducting qubits with opposite-sign anharmonicity, *Phys. Rev. Lett.* **125**, 200503 (2020).

[15] L. Xie, J. Zhai, Z. Zhang, J. Allcock, S. Zhang, and Y.-C. Zheng, Suppressing zz crosstalk of quantum computers through pulse and scheduling co-optimization, in *Proceedings of the 27th ACM International Conference on Architectural Support for Programming Languages and Operating Systems*, ASPLOS '22 (Association for Computing Machinery, New York, NY, USA, 2022) p. 499–513.

[16] Y. Ding, P. Gokhale, S. F. Lin, R. Rines, T. Propson, and F. T. Chong, Systematic crosstalk mitigation for superconducting qubits via frequency-aware compilation, in *2020 53rd Annual IEEE/ACM International Symposium on Microarchitecture (MICRO)* (IEEE, 2020) p. 201–214.

[17] P. Murali, D. C. Mckay, M. Martonosi, and A. Javadi-Abhari, Software mitigation of crosstalk on noisy intermediate-scale quantum computers, in *Proceedings of the Twenty-Fifth International Conference on Architectural Support for Programming Languages and Operating Systems*, ASPLOS '20 (ACM, 2020) p. 1001–1016.

[18] C. Zhang, Y. Chen, Y. Jin, W. Ahn, Y. Zhang, and E. Z. Zhang, Slackq : Approaching the qubit mapping problem with a slack-aware swap insertion scheme (2020), arXiv:2009.02346 [cs.ET].

[19] B. Zhang, S. Majumder, P. H. Leung, S. Crain, Y. Wang, C. Fang, D. M. Debroy, J. Kim, and K. R. Brown, Hidden inverses: Coherent error cancellation at the circuit level, *Phys. Rev. Appl.* **17**, 034074 (2022).

[20] A. R. R. Carvalho, H. Ball, M. J. Biercuk, M. R. Hush, and F. Thomsen, Error-robust quantum logic optimization using a cloud quantum computer interface, *Phys. Rev. Appl.* **15**, 064054 (2021).

[21] A. Seif, H. Liao, V. Tripathi, K. Krsulich, M. Malekakhlagh, M. Amico, P. Jurcevic, and A. Javadi-Abhari, Suppressing correlated noise in quantum computers via context-aware compiling, in *2024 ACM/IEEE 51st Annual International Symposium on Computer Architecture (ISCA)* (IEEE, 2024) p. 310–324.

[22] D. Buterakos, R. E. Throckmorton, and S. Das Sarma, Crosstalk error correction through dynamical decoupling of single-qubit gates in capacitively coupled singlet-triplet semiconductor spin qubits, *Phys. Rev. B* **97**, 045431 (2018).

[23] K. X. Wei, E. Magesan, I. Lauer, S. Srinivasan, D. F. Bogorin, S. Carnevale, G. A. Keefe, Y. Kim, D. Klaus, W. Landers, N. Sundaresan, C. Wang, E. J. Zhang, M. Steffen, O. E. Dial, D. C. McKay, and A. Kandala, Hamiltonian engineering with multicolor drives for fast entangling gates and quantum crosstalk cancellation, *Phys. Rev. Lett.* **129**, 060501 (2022).

[24] V. Tripathi, H. Chen, M. Khezri, K.-W. Yip, E. Levenson-Falk, and D. A. Lidar, Suppression of crosstalk in superconducting qubits using dynamical decoupling, *Phys. Rev. Appl.* **18**, 024068 (2022).

[25] A. F. Brown and D. A. Lidar, Efficient chromatic-number-based multi-qubit decoherence and crosstalk suppression (2024), arXiv:2406.13901 [quant-ph].

[26] P. Coote, R. Dimov, S. Maity, G. S. Hartnett, M. J. Biercuk, and Y. Baum, Resource-efficient context-aware dynamical decoupling embedding for arbitrary large-scale quantum algorithms (2024), arXiv:2409.05962 [quant-ph].

[27] Z. Zhou, R. Sitler, Y. Oda, K. Schultz, and G. Quiroz, Quantum crosstalk robust quantum control, *Phys. Rev. Lett.* **131**, 210802 (2023).

[28] S. J. Beale, J. J. Wallman, M. Gutiérrez, K. R. Brown, and R. Laflamme, Quantum error correction decoheres noise, *Phys. Rev. Lett.* **121**, 190501 (2018).

[29] S. Bravyi, M. Englbrecht, R. König, and N. PEARd, Correcting coherent errors with surface codes, *npj Quantum Information* **4**, 10.1038/s41534-018-0106-y (2018).

[30] D. Greenbaum and Z. Dutton, Modeling coherent errors in quantum error correction, *Quantum Science and Technology* **3**, 015007 (2017).

[31] F. Liu, G. Tang, L. Duan, and Y. Wu, Performance analysis for crosstalk errors between parallel entangling gates in trapped ion quantum error correction (2025), arXiv:2501.09554 [quant-ph].

[32] E. Huang, A. C. Doherty, and S. Flammia, Performance of quantum error correction with coherent errors, *Physical Review A* **99**, 10.1103/physreva.99.022313 (2019).

[33] D. M. Debroy, M. Li, S. Huang, and K. R. Brown, Logical performance of 9 qubit compass codes in ion traps with crosstalk errors (2020), arXiv:1910.08495 [quant-ph].

[34] J. K. Iverson and J. Preskill, Coherence in logical quantum channels, *New Journal of Physics* **22**, 073066 (2020).

[35] N. M. Linke, M. Gutierrez, K. A. Landsman, C. Figgatt, S. Debnath, K. R. Brown, and C. Monroe, Fault-tolerant quantum error detection, *Science Advances* **3**, 10.1126/sciadv.1701074 (2017).

[36] D. Honciuc Menendez, A. Ray, and M. Vasmer, Implementing fault-tolerant non-clifford gates using the $[[8,3,2]]$ color code, *Physical Review A* **109**, 10.1103/physreva.109.062438 (2024).

[37] J. Ku, X. Xu, M. Brink, D. C. McKay, J. B. Hertzberg, M. H. Ansari, and B. L. T. Plourde, Suppression of unwanted zz interactions in a hybrid two-qubit system, *Phys. Rev. Lett.* **125**, 200504 (2020).

[38] J. M. Gambetta, A. D. Córcoles, S. T. Merkel, B. R. Johnson, J. A. Smolin, J. M. Chow, C. A. Ryan, C. Rigetti, S. Poletto, T. A. Ohki, M. B. Ketchen, and M. Steffen, Characterization of addressability by simultaneous randomized benchmarking, *Phys. Rev. Lett.* **109**, 240504 (2012).

[39] P. Zhao, P. Xu, D. Lan, X. Tan, H. Yu, and Y. Yu, Switchable next-nearest-neighbor coupling for controlled two-qubit operations, *Phys. Rev. Appl.* **14**, 064016 (2020).

[40] F. Marxer, A. Vepsäläinen, S. W. Jolin, J. Tuorila, A. Landra, C. Ockeloen-Korppi, W. Liu, O. Ahonen, A. Auer, L. Belzane, V. Bergholm, C. F. Chan, K. W. Chan, T. Hiltunen, J. Hotari, E. Hyypää, J. Ikonen, D. Janzso, M. Koistinen, J. Kotilahti, T. Li, J. Luus, M. Papic, M. Partanen, J. Räbinä, J. Rostila, M. Savitskyi, M. Seppälä, V. Sevriuk, E. Takala, B. Tarasinski, M. J. Thapa, F. Tosto, N. Vorobeva, L. Yu, K. Y. Tan, J. Hassel, M. Möttönen, and J. Heinsoo, Long-distance transmon coupler with cz-gate fidelity above 99.8%, *PRX Quantum* **4**, 010314 (2023).

[41] A. G. Fowler, M. Mariantoni, J. M. Martinis, and A. N. Cleland, Surface codes: Towards practical large-scale quantum computation, *Phys. Rev. A* **86**, 032324 (2012).

[42] D. Horsman, A. G. Fowler, S. Devitt, and R. V. Meter, Surface code quantum computing by lattice surgery, *New*

Journal of Physics **14**, 123011 (2012).

[43] Exponential suppression of bit or phase errors with cyclic error correction, *Nature* **595**, 383–387 (2021).

[44] Suppressing quantum errors by scaling a surface code logical qubit, *Nature* **614**, 676 (2023).

[45] Y. Zhao, Y. Ye, H.-L. Huang, Y. Zhang, D. Wu, H. Guan, Q. Zhu, Z. Wei, T. He, S. Cao, F. Chen, T.-H. Chung, H. Deng, D. Fan, M. Gong, C. Guo, S. Guo, L. Han, N. Li, S. Li, Y. Li, F. Liang, J. Lin, H. Qian, H. Rong, H. Su, L. Sun, S. Wang, Y. Wu, Y. Xu, C. Ying, J. Yu, C. Zha, K. Zhang, Y.-H. Huo, C.-Y. Lu, C.-Z. Peng, X. Zhu, and J.-W. Pan, Realization of an error-correcting surface code with superconducting qubits, *Phys. Rev. Lett.* **129**, 030501 (2022).

[46] C. Gidney, Stim: a fast stabilizer circuit simulator, *Quantum* **5**, 497 (2021).

[47] O. Higgott, Pymatching: A python package for decoding quantum codes with minimum-weight perfect matching (2021), arXiv:2105.13082 [quant-ph].

[48] C. Gidney, Stability experiments: The overlooked dual of memory experiments, *Quantum* **6**, 786 (2022).

[49] G. P. Gehér, M. Jastrzebski, E. T. Campbell, and O. Crawford, To reset, or not to reset – that is the question (2024), arXiv:2408.00758 [quant-ph].

[50] D. Litinski, A game of surface codes: Large-scale quantum computing with lattice surgery, *Quantum* **3**, 128 (2019).

[51] C. Chamberland and E. T. Campbell, Universal quantum computing with twist-free and temporally encoded lattice surgery, *PRX Quantum* **3**, 010331 (2022).

[52] H. Bombín, C. Dawson, R. V. Mishmash, N. Nickerson, F. Pastawski, and S. Roberts, Logical blocks for fault-tolerant topological quantum computation, *PRX Quantum* **4**, 020303 (2023).

[53] R. Chao and B. W. Reichardt, Flag fault-tolerant error correction for any stabilizer code, *PRX Quantum* **1**, 010302 (2020).

[54] R. Chao and B. W. Reichardt, Fault-tolerant quantum computation with few qubits, *npj Quantum Information* **4**, 10.1038/s41534-018-0085-z (2018).

[55] R. Chao and B. W. Reichardt, Quantum error correction with only two extra qubits, *Physical Review Letters* **121**, 10.1103/physrevlett.121.050502 (2018).